

Nearly Perfect Single-Channel Conduction in Disordered Armchair Nanoribbons

Masayuki Yamamoto¹, Yositake Takane¹, and Katsunori Wakabayashi^{1,2}

¹*Department of Quantum Matter, AdSM, Hiroshima University, Higashi-Hiroshima 739-8530, Japan and*

²*PRESTO, Japan Science and Technology Agency(JST), Kawaguchi 332-0012, Japan*

(Dated: October 31, 2018)

The low-energy spectrum of graphene nanoribbons with armchair edges (armchair nanoribbons) is described as the superposition of two non-equivalent Dirac points of graphene. In spite of the lack of well-separated two valley structures, the single-channel transport subjected to long-ranged impurities is nearly perfectly conducting, where the backward scattering matrix elements in the lowest order vanish as a manifestation of internal phase structures of the wavefunction. For multi-channel energy regime, however, the conventional exponential decay of the averaged conductance occurs. Since the inter-valley scattering is not completely absent, armchair nanoribbons can be classified into orthogonal universality class irrespective of the range of impurities. The nearly perfect single-channel conduction dominates the low-energy electronic transport in rather narrow nanoribbons.

PACS numbers: 72.10.-d,72.15.Rn,73.20.At,73.20.Fz,73.23.-b

I. INTRODUCTION

Graphene is the first true two-dimensional (2D) material¹. Due to the honeycomb lattice structure of sp^2 carbon, the π electronic states near the Fermi energy behave as the massless Dirac fermions. This leads to many nontrivial properties of graphene such as half-integer quantum Hall effect². The valence and conduction bands touch conically at two non-equivalent Dirac points, called K_+ and K_- points, which possess opposite chirality³. In graphene, the presence of edges can have strong implications for the electronic band structure of π electrons^{4,5,6}. Graphene nanoribbons (GNR) with zigzag edges are known to have partial flat bands near the Fermi energy due to the edge localized states. The electronic structures of nanoribbons with armchair edges crucially depend on the ribbon width^{4,5,6,7}. Recent rapid progress of experiments confirmed the edge-dependent electronic states of graphene using scanning tunneling microscope^{8,9}, and also succeeded in creating GNR using lithographic¹⁰ or chemical techniques¹¹.

GNR displays unusual electronic transport properties, in apparent conflict with the common belief that 1D systems are generally subject to Anderson localization. Indeed it was demonstrated that nanoribbons with zigzag edges (zigzag nanoribbons) with long-ranged impurities possess one perfectly conducting channel (PCC), *i.e.* the absence of Anderson localization^{12,13}. Since in zigzag nanoribbons the propagating modes in each valley contain a single chiral mode originating from edge states, a single PCC emerges, associated with such a chiral mode, if the impurity scattering does not connect the two valleys, *i.e.* for long-ranged impurities (LRI).

In this paper, we show that the single-channel transport in the disordered armchair nanoribbons subjected to the long-ranged impurities is nearly perfectly conducting in spite of the lack of well-separated two valley structures. The origin of the nearly perfect conduction is the cancellation of the backward scattering matrix elements in the lowest order due to the manifestation of internal

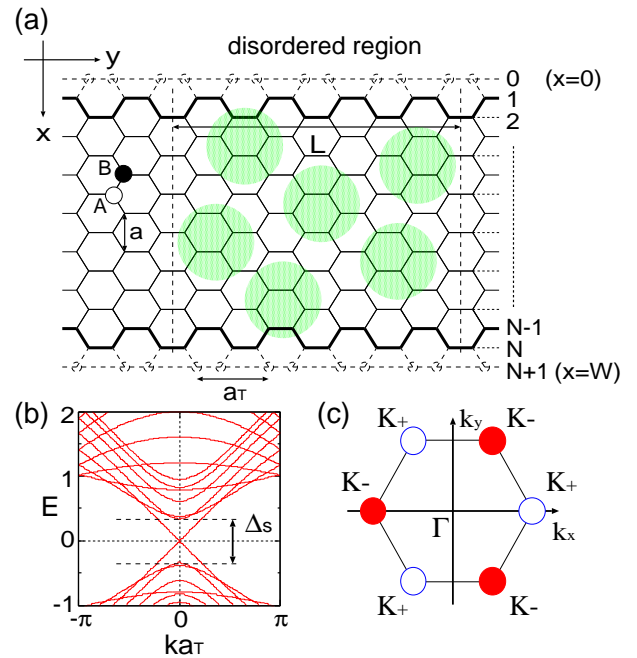


FIG. 1: (a) Structure of graphene armchair nanoribbon. The area with the length L represents the disordered region with randomly distributed impurities. (b) Energy dispersion of armchair ribbon with $N = 14$. The energy range for single-channel transport is described by Δ_s . (c) 1st Brillouin Zone of graphene.

phase structures of the wavefunction. For multi-channel energy regime, however, the conventional exponential decay of the averaged conductance occurs. Since the inter-valley scattering is not completely absent, the disordered armchair nanoribbons can be classified into orthogonal class. The nearly perfectly conducting effect dominates the low-energy electronic transport properties in rather narrow nanoribbons.

The paper is organized as follows: In Sec. II, the tight-

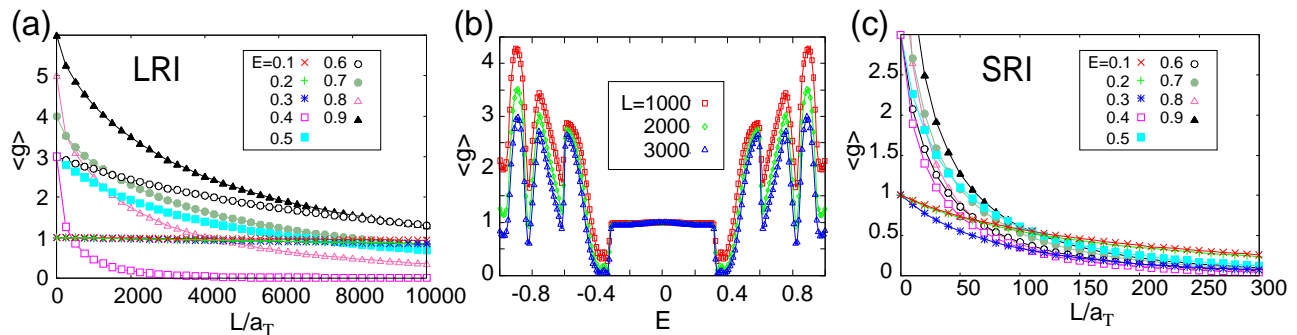


FIG. 2: (a) Average conductance $\langle g \rangle$ as a function of the ribbon length L in the presence of long-ranged impurities (LRI) for several different Fermi energies E . Conductance is almost unaffected by impurities for single-channel transport ($E = 0.1, 0.2$ and 0.3) while it shows a conventional exponential decay for multi-channel transport ($E \geq 0.4$). Here, $N = 14$, $n_{\text{imp.}} = 0.1$ and $d/a = 1.5$. Ensemble average is taken over 10^4 samples. (b) The Fermi energy dependence of $\langle g \rangle$ for LRI. (c) The same as (a) for short-ranged impurities (SRI). Here, $N = 14$, $n_{\text{imp.}} = 0.1$ and $d/a = 0.1$.

binding model used in our numerical simulation is explained. We also briefly review the electronic states of the low-energy single channel mode in armchair nanoribbons by $\mathbf{k} \cdot \mathbf{p}$ scheme. In Sec. III, we present the numerical results indicating the nearly perfect single-channel conduction. This property is then explained by T -matrix analysis. Symmetry consideration is also given in this section. Finally we summarize our work in Sec. IV.

II. ELECTRONIC STATES OF ARMCHAIR NANORIBBONS

A. Tight-binding model

We describe the electronic states of graphene nanoribbons with armchair edges by the tight-binding model

$$H = \sum_{\langle i,j \rangle} \gamma_{ij} c_i^\dagger c_j + \sum_i V_i c_i^\dagger c_i, \quad (1)$$

where c_i (c_i^\dagger) denotes the creation (annihilation) operator of an π -electron on the site i neglecting the spin degree of freedom. $\gamma_{ij} = -1$ if i and j are nearest neighbors, and 0 otherwise. In the following we will also apply magnetic fields perpendicular to the graphite plane which are incorporated via the Peierls phase: $\gamma_{ij} \rightarrow \gamma_{ij} \exp \left[i2\pi(e/ch) \int_i^j d\mathbf{l} \cdot \mathbf{A} \right]$, where \mathbf{A} is the vector potential. The second term in Eq. (1) represents the impurity potential, $V_i = V(\mathbf{r}_i)$, at position \mathbf{r}_i .

In Fig. 1(a), the schematic figure of armchair ribbons is depicted. The ribbon width N is defined by the number of zigzag kinks in the transverse direction. The armchair ribbon can be metallic if $N = 3m - 1$ (m : integer number) as shown in Fig. 1(b), otherwise semiconducting. The disordered sample region with the length L is attached to two reservoirs via semi-infinite ideal regions.

We assume that impurities are randomly distributed with density $n_{\text{imp.}}$. Each impurity potential has the

Gaussian form of range d ,

$$V_i = V(\mathbf{r}_i) = \sum_{\mathbf{r}_0(\text{random})} u \exp \left(-\frac{|\mathbf{r}_i - \mathbf{r}_0|^2}{d^2} \right), \quad (2)$$

where the strength u is uniformly distributed within the range $|u| \leq u_M$. Here u_M satisfies the normalization condition: $u_M \sum_{\mathbf{r}_i}^{\text{(fullspace)}} \exp(-\mathbf{r}_i^2/d^2) / (\sqrt{3}/2) = u_0$. In this work, we set $n_{\text{imp.}} = 0.1$, $u_0 = 1.0$ and $d/a = 1.5$ for LRI and $d/a = 0.1$ for short-ranged impurities (SRI).

B. Low-energy single channel mode

Here we briefly review the relation between the low-energy electronic states of armchair nanoribbons and the Dirac spectrum of graphene. The electronic states near the Dirac point in graphene can be described by the massless Dirac Hamiltonian

$$\hat{H}_0 = \tilde{\gamma} \left[\hat{k}_x (\sigma^x \otimes \tau^0) - \hat{k}_y (\sigma^y \otimes \tau^z) \right], \quad (3)$$

acting on the 4-component pseudospinor envelope functions $\mathbf{F}(\mathbf{r}) = [F_A^+(\mathbf{r}), F_B^+(\mathbf{r}), F_A^-(\mathbf{r}), F_B^-(\mathbf{r})]$, which characterize the wave functions on the two crystalline sublattices (A and B) for the two non-equivalent Dirac points (valleys) \mathbf{K}_\pm shown in Fig. 1(c). The corresponding wave vector for the \mathbf{K}_+ point is $\mathbf{K} = (2\pi/a)(2/3, 0)$, and that for the \mathbf{K}_- point is $-\mathbf{K}$. We have defined the amplitude of wavefunction at \mathbf{R}_A and that at \mathbf{R}_B as $\psi_A(\mathbf{R}_A) = e^{i\mathbf{K} \cdot \mathbf{R}_A} F_A^+(\mathbf{R}_A) + e^{-i\mathbf{K} \cdot \mathbf{R}_A} F_A^-(\mathbf{R}_A)$ and $\psi_B(\mathbf{R}_B) = e^{i\mathbf{K} \cdot \mathbf{R}_B} F_B^+(\mathbf{R}_B) - e^{-i\mathbf{K} \cdot \mathbf{R}_B} F_B^-(\mathbf{R}_B)$, respectively. Here, \mathbf{R}_A (\mathbf{R}_B) is the coordinate of an arbitrary \mathbf{A} (\mathbf{B}) sublattice site. Here $\tilde{\gamma}$ is the band parameter, \hat{k}_x (\hat{k}_y) are wave number operators, and τ^0 is the 2×2 identity matrix. Pauli matrices $\sigma^{x,y,z}$ act on the sublattice space (A, B), while $\tau^{x,y,z}$ on the valley space (\mathbf{K}_\pm). The boundary condition for armchair nanoribbons¹⁴ can

be written as

$$[F_A^+(x, y) + F_A^-(x, y)]|_{x=0, W} = 0, \quad (4)$$

$$[F_B^+(x, y) - F_B^-(x, y)]|_{x=0, W} = 0. \quad (5)$$

Since this boundary condition projects \mathbf{K}_+ and \mathbf{K}_- states into Γ point in the first Brillouin Zone as seen in Fig. 1(c), the low-energy states for armchair nanoribbons are the superposition of \mathbf{K}_+ and \mathbf{K}_- states. If the ribbon width W satisfies the condition of $W = (3/2)(N_w + 1)a$ with $N_w = 0, 1, 2, \dots$, the system becomes metallic with the linear spectrum. The corresponding energy is given by

$$\epsilon_{n, k, s} = s\tilde{\gamma}\sqrt{\kappa_n^2 + k^2}, \quad (6)$$

where $\kappa_n = \frac{2\pi n}{3(N_w + 1)a}$, $n = 0, \pm 1, \pm 2, \dots$ and $s = \pm$. The $n = 0$ mode is the lowest linear subband for metallic armchair ribbons. The energy gap (Δ_s) to first parabolic subband of $n = 1$ is given as

$$\Delta_s = 4\pi\tilde{\gamma}/3(N_w + 1)a, \quad (7)$$

which is inversely proportional to ribbon width. It should be noted that small energy gap can be acquired due to the Peierls distortion for half-filling at low temperatures^{7,15}, but such effect is not relevant for single-channel transport in the doped energy regime.

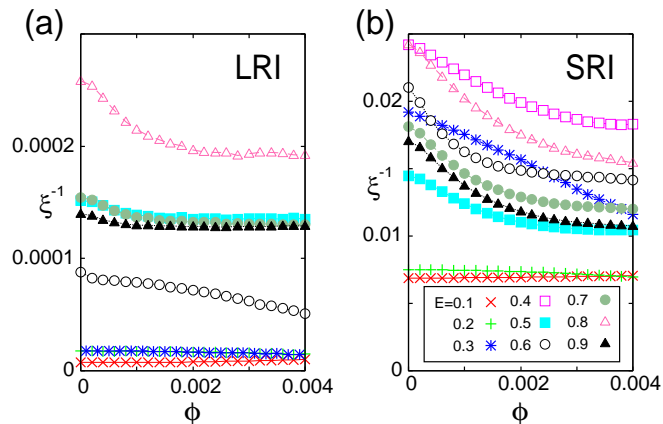


FIG. 3: Inverse of localization length ξ^{-1} as a function of the magnetic flux ϕ through a hexagon ring measured in units of ch/e , in the presence of (a) LRI and (b) SRI for different Fermi energies E . In (a), ξ^{-1} for $E = 0.4$ is omitted since its value is much larger than others.

III. ELECTRONIC TRANSPORT PROPERTIES OF DISORDERED NANORIBBONS

A. Numerical simulation

Now we turn to the discussion of the electronic transport properties of disordered nanoribbons. We evaluate

the dimensionless conductance by using the Landauer formula, $g(E) = \text{Tr}(\mathbf{t}^\dagger \mathbf{t})$. Here the transmission matrix $\mathbf{t}(E)$ for disordered system is calculated by using the recursive Green function method¹⁶.

Figure 2(a) shows the averaged conductance $\langle g \rangle$ as a function of the ribbon length L in the presence of LRI for several different Fermi energies E . As we can clearly see, the averaged conductance subjected to LRI in the single-channel transport ($E = 0.1, 0.2$ and 0.3) is nearly equal to one even in the long wire regime. This result is contrary to our expectation that electrons are scattered even by LRI, since wavefunctions at \mathbf{K}_+ and \mathbf{K}_- points are mixed in armchair ribbons. For multi-channel transport ($E \geq 0.4$), the conductance shows a conventional decay. The robustness of single-channel transport can be clearly viewed from the Fermi energy dependence of conductance for several different ribbon lengths L as shown in Fig. 2(b). It should be noted that the energy dependence in the vicinity of $E = 0$ is quite different from that in zigzag nanoribbons. The conductance decays rapidly due to the finite ribbon width effect in zigzag ribbons¹² while the conductance around $E = 0$ remains unity in armchair ribbons (Fig. 2(b)).

Now let us see the effect of short-ranged impurities (SRI). Figure 2(c) shows the average conductance $\langle g \rangle$ as a function of the ribbon length L in the presence of SRI for several different Fermi energies E . In this case, the conductance decays exponentially even for single-channel transport. This result is similar to that previously obtained in zigzag ribbons. However, the rate of decay in the low-energy single-channel regime ($E = 0.1$ and 0.2) is slower than that for multi-channel transport regime ($E \geq 0.4$) in this case. Similar results are obtained in Ref.¹⁷, but in which only short-ranged disorder at edge of ribbon is considered.

B. T -matrix analysis

The absence of localization in the single-channel region can be understood from the Dirac equation including the impurity potential term \hat{U}_{imp} with armchair edge boundary. To consider the amplitude of backward scattering, we introduce the T -matrix defined as

$$T = \hat{U}_{\text{imp}} + \hat{U}_{\text{imp}} \frac{1}{E - \hat{H}_0} \hat{U}_{\text{imp}} + \dots \quad (8)$$

According to Ref.¹⁸, \hat{U}_{imp} is written as

$$\hat{U}_{\text{imp}} = \begin{pmatrix} u_A(\mathbf{r}) & 0 & u'_A(\mathbf{r}) & 0 \\ 0 & u_B(\mathbf{r}) & 0 & -u'_B(\mathbf{r}) \\ u'_A(\mathbf{r})^* & 0 & u_A(\mathbf{r}) & 0 \\ 0 & -u'_B(\mathbf{r})^* & 0 & u_B(\mathbf{r}) \end{pmatrix}, \quad (9)$$

with

$$u_X(\mathbf{r}) = \sum_{\mathbf{R}_X} g(\mathbf{r} - \mathbf{R}_X) \tilde{u}_X(\mathbf{R}_X), \quad (10)$$

$$u'_X(\mathbf{r}) = \sum_{\mathbf{R}_X} g(\mathbf{r} - \mathbf{R}_X) e^{-i2\mathbf{K} \cdot \mathbf{R}_X} \tilde{u}_X(\mathbf{R}_X), \quad (11)$$

where $\tilde{u}_X(\mathbf{R}_X)$ is the local potential due to impurities for $X = A$ or B . Here $g(\mathbf{R})$ with the normalization condition of $\sum_{\mathbf{R}} g(\mathbf{R}) = 1$ is the real function which has an appreciable amplitude in the region where $|\mathbf{R}|$ is smaller than a few times of the lattice constant, and decays rapidly with increasing $|\mathbf{R}|$. If only the LRI are present, we can approximate $u_A(\mathbf{r}) = u_B(\mathbf{r}) \equiv u(\mathbf{r})$ and $u'_A(\mathbf{r}) = u'_B(\mathbf{r}) \equiv u'(\mathbf{r})$. In the case of carbon nanotubes and zigzag nanoribbons, $u'_X(\mathbf{r})$ vanishes after the summation over \mathbf{R}_X in Eq. (11) since the phase factor $e^{-i2\mathbf{K} \cdot \mathbf{R}_X}$ strongly oscillates in the x -direction. However, this cancellation is not complete in an armchair nanoribbon because the averaging over the x -direction is restricted to the finite width of W . This means that we cannot neglect the contribution from scatterers particularly in the vicinity of the edges to $u'_X(\mathbf{r})$. Although $u'_X(\mathbf{r})$ becomes small after the summation, the symmetry of system changes for $u'_X(\mathbf{r}) \neq 0$ as we will see in the next subsection.

Now we evaluate the matrix elements of \hat{U}_{imp} for the eigenstate $|n, k, s\rangle$ with the eigen energy of Eq. (6) which can be written as

$$|n, k, s\rangle = \frac{1}{\sqrt{4WL}} \left(\begin{array}{c} s \\ e^{-i\theta(n,k)} \end{array} \right) e^{i\kappa_n x} \left(\begin{array}{c} -s \\ e^{-i\theta(n,k)} \end{array} \right) e^{-i\kappa_n x} e^{iky}, \quad (12)$$

with the phase factor

$$e^{-i\theta(n,k)} = \frac{\kappa_n - ik}{\sqrt{\kappa_n^2 + k^2}}. \quad (13)$$

Here it should be noted that the phase structure in Eq. (12) is different between \mathbf{K}_+ and \mathbf{K}_- states, and this internal phase structures are critical for the scattering matrix elements of armchair nanoribbons as we discuss in the following. Using the above expression, we can obtain the scattering matrix element

$$\begin{aligned} \langle n, k, s | \hat{U}_{\text{imp}} | n', k', s' \rangle &= \left(s s' + e^{i(\theta(n,k) - \theta(n',k'))} \right) \\ &\times V(n, k; n', k'), \end{aligned} \quad (14)$$

with

$$\begin{aligned} V(n, k; n', k') &= \frac{1}{4WL} \int_0^W dx \int_0^L dy e^{-i(k-k')y} \\ &\times \left[u(\mathbf{r}) \left(e^{-i(\kappa_n - \kappa_{n'})x} + \text{c.c.} \right) \right. \\ &\left. - \left(u'(\mathbf{r}) e^{-i(\kappa_n + \kappa_{n'})x} + \text{c.c.} \right) \right]. \end{aligned} \quad (15)$$

It should be emphasized that Eq. (14) has the same form as that obtained for carbon nanotubes without inter-valley scattering ($u'_X(\mathbf{r}) = 0$)¹⁸. Interestingly, in spite of the fact that armchair nanoribbons inevitably suffer from the inter-valley scattering due to the armchair edges ($u'_X(\mathbf{r}) \neq 0$), we can express the matrix element for the backward scattering as Eq. (14) by including $u'_X(\mathbf{r})$ into $V(n, k; n', k')$ in Eq. (15). This is due to the different phase structure between \mathbf{K}_+ and \mathbf{K}_- in Eq. (12).

We focus on the single-channel regime where only the lowest subband with $n = 0$ crosses the Fermi level. From Eq. (14), the scattering amplitude from the propagating state $|0, k, s\rangle$ to its backward state $|0, -k, s\rangle$ in the single-channel mode becomes identically zero, *i.e.*

$$\langle 0, -k, s | \hat{U}_{\text{imp}} | 0, k, s \rangle = 0. \quad (16)$$

Thus, since the lowest backward scattering matrix element of T -matrix vanishes, the decay of $\langle g \rangle$ in the single channel energy regime is extremely slow as a function of the ribbon length as we have seen in Fig. 2. However, the back-scattering amplitude in the second and much higher order does not vanish. Hence the single-channel conduction is not exactly perfect like carbon nanotubes¹⁸, but *nearly* perfect in armchair nanoribbons.

The present results of nearly perfect single-channel transport might be similar to those obtained in carbon nanotubes by solving the Boltzmann transport equation, which is valid for incoherent systems in the absence of inter-valley scattering¹⁹. However, our results are for the coherent system with inter-valley scattering by armchair edge and their physical mechanism is different.

C. Symmetry consideration

Now we give a symmetry consideration to disordered graphene and graphene nanoribbons. If the inter-valley scattering is absent, *i.e.* $u'_X(\mathbf{r}) = 0$, the Hamiltonian $\hat{H}_0 + \hat{U}_{\text{imp}}$ becomes invariant under the transformation of $\mathcal{S} = -i(\sigma^y \otimes \tau^0) C$, where C is the complex-conjugate operator. This operation corresponds to the special time-reversal operation for pseudospins within each valley, and supports that the system has the symplectic symmetry. However, in the presence of inter-valley scattering due to SRI, the invariance under \mathcal{S} is broken. In this case, the time reversal symmetry across two valleys described by the operator $\mathcal{T} = (\sigma^z \otimes \tau^x) C$ becomes relevant, which indicates orthogonal universality class. Thus as noted in Ref.²⁰, graphene with LRI belongs to symplectic symmetry, but that with SRI belongs to orthogonal symmetry.

However, in the disordered armchair ribbons, the special time-reversal symmetry within each valley is broken even in the case of LRI. This is because $u'_X(\mathbf{r}) \neq 0$ as we have seen in the previous subsection. Thus, irrespective of the range of impurities, the armchair ribbons are classified into orthogonal universality class. Actually, the application of magnetic field shows rather

strong magnetic field dependence on the inverse localization length in the regime of the weak magnetic field for both LRI and SRI cases (Fig. 3). This is consistent with the behavior of orthogonal universality class. Here, the inverse localization length is evaluated by identifying $\exp(\ln g) = \exp(-L/\xi)$. Since the disordered zigzag nanoribbons are classified into unitary class for LRI but orthogonal class for SRI¹², it should be noted that the universality crossover in nanographene system can occur not only due to the range of impurities but also due to the edge boundary conditions.

IV. SUMMARY

In this work, we have numerically investigated the electronic transport in disordered armchair nanoribbons in the presence of short- and long-ranged impurities. In spite of the lack of well-separated two valley structures, the single-channel transport subjected to long-ranged impurities shows nearly perfect transmission, where the

backward scattering matrix elements in the lowest order vanish as a manifestation of internal phase structures of the wavefunction. These results are contrast with the mechanism of perfectly conducting channel in disordered zigzag nanoribbons and metallic nanotubes where the well separation between two non-equivalent Dirac points is essential to suppress the inter-valley scattering. Within the Born approximation, this cancellation is satisfied even for SRI, which can be clearly seen in Fig. 2(b). The dependency of conductance on the Fermi energy confirms our calculation about the difference between single- and multi-channel transport properties. The symmetry consideration classifies the armchair nanoribbons into orthogonal class.

Acknowledgement

This work was financially supported by a Grand-in-Aid for Scientific Research from the MEXT and the JSPS (Nos. 19710082, 19310094 and 20001006).

-
- ¹ K. S. Novoselov, A.K. Geim, S.V. Morozov, D. Jiang, S.V. Dubonos, I.V. Grigorieva and A.A. Firsov, *Science* **306**, 666 (2004).
- ² K. S. Novoselov, A.K. Geim, S.V. Morozov, D. Jiang, M.I. Katsnelson, I.V. Grigorieva, S.V. Dubonos and A.A. Firsov, *Nature* **438**, 197 (2005).
- ³ A. H. Castro Neto, F. Guinea and N.M.R. Peres, *Phys. Rev. B* **73**, 205408 (2006).
- ⁴ M. Fujita, K. Wakabayashi, K. Nakada and K. Kusakabe, *J. Phys. Soc. Jpn.* **65**, 1920 (1996).
- ⁵ K. Nakada, M. Fujita, G. Dresselhaus and M.S. Dresselhaus, *Phys. Rev. B* **54**, 17954 (1996).
- ⁶ K. Wakabayashi, M. Fujita, H. Ajiki and M. Sigrist, *Phys. Rev. B* **59**, 8271 (1999).
- ⁷ Y.-W. Son, M.L. Cohen and S.G. Louie, *Phys. Rev. Lett.* **97**, 216803 (2006).
- ⁸ Y. Niimi, T. Matsui, H. Kambara, K. Tagami, M. Tsukada and H. Fukuyama, *Phys. Rev. B* **73**, 085421 (2006).
- ⁹ Y. Kobayashi, K. Fukui, T. Enoki, K. Kusakabe and Y. Kaburagi, *Phys. Rev. B* **71**, 193406 (2005).
- ¹⁰ M.Y. Han, B. Özyilmaz, Y. Zhang and P. Kim, *Phys. Rev. Lett.* **98**, 206805 (2007).
- ¹¹ X. Li, X. Wang, L. Zhang, S. Lee and H. Dai, *Science* **319**, 1229 (2008).
- ¹² K. Wakabayashi, Y. Takane and M. Sigrist, *Phys. Rev. Lett.* **99**, 036601 (2007).
- ¹³ K. Wakabayashi, Y. Takane, M. Yamamoto and M. Sigrist, *CARBON* **47**, 124 (2009).
- ¹⁴ L. Brey and H.A. Fertig, *Phys. Rev. B* **73**, 235411 (2006).
- ¹⁵ M. Fujita, M. Igami and K. Nakada, *J. Phys. Soc. Jpn.* **66**, 1864 (1997).
- ¹⁶ T. Ando, *Phys. Rev. B* **44**, 8017 (1991).
- ¹⁷ T. C. Lin and S.-P. Lu, *Phys. Rev. B* **77**, 085408 (2008).
- ¹⁸ T. Ando and T. Nakanishi, *J. Phys. Soc. Jpn.* **67**, 1704 (1998).
- ¹⁹ T. Ando and H. Suzuura, *J. Phys. Soc. Jpn.* **71**, 2753 (2002).
- ²⁰ H. Suzuura and T. Ando, *Phys. Rev. Lett.* **89**, 266603 (2002).